Rapid Communications

Mott-Hubbard gaps and their doping-induced collapse in strongly correlated pyrochlore ruthenates

R. Kaneko [1,2] K. Ueda [1] C. Terakura,[2] and Y. Tokura[1,2,3]
[1]*Department of Applied Physics, University of Tokyo, Tokyo 113-8656, Japan*
[2]*RIKEN Center for Emergent Matter Science (CEMS), Wako 351-0198, Japan*
[3]*Tokyo College, University of Tokyo, Tokyo 113-8656, Japan*

(Received 1 May 2020; revised 2 July 2020; accepted 2 July 2020; published 17 July 2020)

We investigate the variation of charge dynamics in the course of the filling-control metal-insulator transitions (MITs) for pyrochlore $R_2Ru_2O_7$ (R being rare-earth ions). With widely changing of R ions from Lu to Pr, the antiferromagnetic transition temperature systematically increases while the magnitude of the charge gap decreases toward zero at the hypothetical bandwidth-control Mott transition. It is attributable to the reduction of effective electron correlation in the Mott-Hubbard insulator regime. Doping holes give rise to the filling-control MITs from antiferromagnetic insulators to paramagnetic metals accompanied by the collapse of the Mott-Hubbard gaps. The doping-induced spectral weight transfer of the optical conductivity from the above-gap region to the in-gap region is nearly proportional to the doping level, whose rate is enhanced with the reduction of the electron correlation, in accord with the standard Mott criticality.

DOI: 10.1103/PhysRevB.102.041114

Metal-insulator transition (MIT) or Mott transition has been a subject of extensive research on the strongly correlated d-electron systems. The Mott transition can be categorized into two types: one is the bandwidth-control MIT and the other is the filling-control MIT, both strongly coupled with magnetism and sometimes with d-electron orbital degrees of freedom [1]. The bandwidth-control MIT is driven by the change of the electron hopping interaction (t) or one-electron bandwidth (W), whereas the filling-control MIT by the change of the electron band filling through the charge doping procedure on the parent Mott insulator. For d-electron transition-metal oxides, the perovskite (ABO_3) or pyrochlore ($A_2B_2O_7$) related complex-oxide structures are convenient for studying filling-control transitions since the chemical substitution procedures of the so-called A site with different-valence ions can change the band filling or promote the doping, as exemplified by the cuprate high-temperature superconductors [2] and colossal magnetoresistance manganites [3]. Recent studies on MITs are extending from the 3d- toward 4d- and 5d-electron systems where the interplay between the electron correlation and the relativistic spin-orbit coupling is anticipated to bring about even more intriguing properties and electronic functions, e.g., magnetism (strong correlation) related topological quantum phenomena. One such example is the emergence of antiferromagnetic Weyl semimetal states near the Mott transition in pyrochlore compounds $R_2Ir_2O_7$ [4,5].

The target of this study is 4d-electron based pyrochlores $R_2Ru_2O_7$, whose crystal structure is depicted in Fig. 1(a), with R being trivalent rare-earth or Y ions. Due to the local trigonal distortions, the t_{2g} orbitals split into the lower nondegenerate a_{1g} orbital and the upper doubly degenerate e'_g orbital. A family of ruthenates $R_2Ru_2O_7$, in which two of four Ru-4d electrons occupy the a_{1g} state and the other two fill in the e'_g state [Fig. 1(b)], show antiferromagnetic orders at low temperatures while electrically insulating in the whole temperature region [6,7]. The magnetic configuration on this geometrically frustrated system has been still under debate. However, the existence of the antiferromagnetic long-range order is clearly confirmed by recent neutron-diffraction studies [7,8] although the spin-glass-like nature is discerned in the magnetization data, as pointed out by early studies [6]. As shown in Fig. 1(c), it is proposed to be a noncollinear or "all-in all-out" type structure with zero net magnetization within each Ru tetrahedra ($\Sigma \boldsymbol{S}_i = 0$) to minimize the total exchange interaction energy [9–11]. This is in contrast with the case of their perovskite analogs with the similar Ru^{4+} valence state, $SrRuO_3$ and $CaRuO_3$, which are ferromagnetic and paramagnetic metals, respectively. This is partly because W of pyrochlore is less than that of perovskite due to the more distorted Ru-O-Ru bonds, hence giving rise to the larger electron correlation U/W, U representing here the on-site Coulomb repulsion energy. One of the major advantages of studying Ru-based pyrochlores is that we can explore the filling-control MIT via the chemical doping on the A (R ion in this case) sites. Actually, the divalent A ion compounds with nominal Ru^{5+} valence (three 4d electrons), such as A = Ca, Cd, and Hg, are reported to exhibit metallic or relatively conductive transport properties which are affected to some extent by magnetic orderings [12–14]. It is in stark contrast to trivalent-R parent compounds. Moreover, the geometrically frustrated lattice of the pyrochlore may also provide a unique opportunity to explore the exotic electronic phase with the Mott criticality and the spin-orbit interaction. These features imply that there can be abundant electronic/magnetic phases in pyrochlore ruthenates by controlling electron counts in Ru-4d orbitals.

In this Rapid Communication, we report a systematic investigation on the charge dynamics in the course of bandwidth- and filling-control MITs in $R_2Ru_2O_7$ by

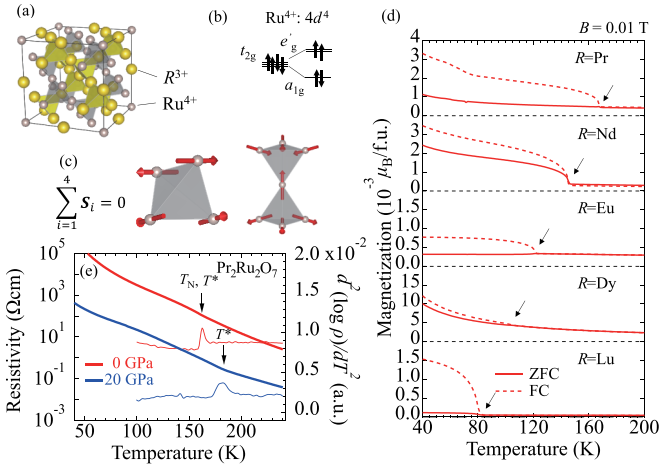

FIG. 1. (a) Crystal structure of $R_2Ru_2O_7$. (b) t_{2g} electronic levels of Ru^{4+} $4d$ state. (c) Examples for possible Ru-$4d$ spin configurations, in which the sum of spin moments within a tetrahedron is zero ($\Sigma \boldsymbol{S}_i = 0$). The right figure shows the all-in all-out state, as one such example. (d) Temperature dependence of magnetization for R = Pr, Nd, Eu, Dy, Lu compounds. Solid (dashed) lines represent the results measured after the zero-field-cooling (ZFC) process [field-cooling (FC)]. The black arrows denote the antiferromagnetic transition T_N. (e) Temperature (T) dependence of resistivity ρ for R = Pr under the pressure $P = 0$ GPa (red bold curve) and 20 GPa (blue bold curve). Thin lines show the second derivative of log ρ. The black arrows indicate the kink position (T^*) of ρ.

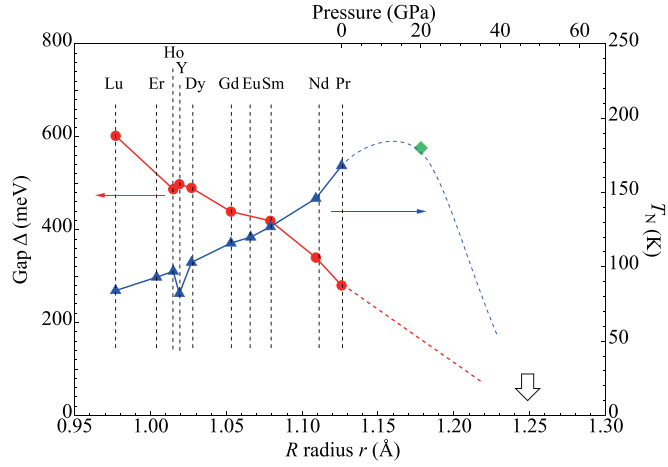

FIG. 2. The Néel temperature T_N (blue triangles) and the magnitude of the charge gap Δ (red circles) measured at 10 K as a function of R ionic radius r. The green square represents T^* estimated in Fig. 1(e). The upper scale for the hydrostatic pressure P on $Pr_2Ru_2O_7$ is calculated by an empirical relation between P and r observed in $R_2Ir_2O_7$.

measurements of optical conductivity spectra and charge transport. The R-site ionic radius (r) in the pyrochlore structure modifies t or W through a change in the Ru-O-Ru bond angle, in analogy to the case of perovskites [1]. As r increases, or equivalently as the effective correlation U/W is weakened, the magnitude of the charge gap decreases while T_N increases. The application of external pressure, which is anticipated to reduce U/W, enhances T_N as well, indicating that the magnetic order can be well described with the strong electron-correlation picture where the superexchange interaction, being proportional to t^2/U, is predominantly at work. We observe that the hole doping drives the insulator-to-metal transitions accompanied by the systematic closing of the charge gap. Our quantitative analysis reveals that the feature of gap closing for R = Pr and Gd with low hole-doping level is accompanied by the spectral weight transfer from the Mott-Hubbard gap excitation, which shows the critical behavior with respect to the effective electron correlation U/W.

The polycrystalline samples of $(R_{1-x}A_x)_2Ru_2O_7$ were prepared with R = Pr-Lu and A = Ca, Cd. All samples were synthesized under 3 GPa and 1200 °C enclosed with pelletized oxidizer $KClO_4$ by using a cubic-anvil-type high-pressure apparatus. Obtained samples were dense and solid enough to accurately and reproducibly measure resistivity and optical reflectivity. We confirmed by powder x-ray diffraction that all samples show a single phase except for a negligible amount of RuO_2 impurity phase whose volume fractions were estimated at less than 1%. For the resistivity measurement under high hydrostatic pressure, we utilized a cubic-anvil-type high-pressure cryostat [15,16]. The optical conductivity spectra were obtained by Kramers-Kronig transformation of the reflectivity spectra, measured in the temperature range from 10 to 300 K and energy range from 0.005 to 5 eV by Fourier transform- and grating-type spectrometers. For accurate Kramers-Kronig transformation, the reflectivity data above 5 eV up to 40 eV, which are to be combined with the lower-energy (<0.5 eV) temperature-dependent reflectivity spectra, were measured at room temperature by using synchrotron radiation at UV-SOR, Institute for Molecular Science.

Figure 1(d) shows the temperature dependence of the magnetization for the compounds with R = Pr, Sm, Eu, Dy, and Lu. The magnetization curves in the field-cooling process exhibit a sharp increase deviating from that in the zero-field-cooling process below T_N. We plot T_N as a function of r in Fig. 2; the observed variation that T_N decreases with decreasing r ($\propto W$) well coincides with the reported one [7]. To access even a wider range of W, we utilize the hydrostatic pressure which is known to increase W. Figure 1(e) shows the temperature dependence of resistivity ρ for R = Pr at the pressure $P = 0$ and 20 GPa, respectively. ρ shows a kink at a finite temperature T^*, which can be seen more clearly in the second derivative of log ρ with T. In fact, T^* is found to coincide with T_N at 0 GPa, and hence can be regarded as another indicator of the magnetic transition, as often done for semiconducting correlated oxides which undergo the magnetic phase transitions [17,18]. T^* is enhanced up to 180 K at $P = 20$ GPa, in accord with a large reduction of ρ. Since the ionic radius of Ru is close to that of Ir in the respective pyrochlores, we tentatively assume the empirical scaling rule between P and r revealed for $R_2Ir_2O_7$ in Ref. [16], that is, $\Delta P = 3.8$ GPa corresponds to $\Delta r = 0.01$ Å. We plot T^* with a green marker in Fig. 2, which reasonably falls onto the extrapolated curve of the observed T_N. The observed r dependence of T_N ($\sim T^*$) indicates that a series of pyrochlore ruthenates belong to the strongly correlated regime, where the

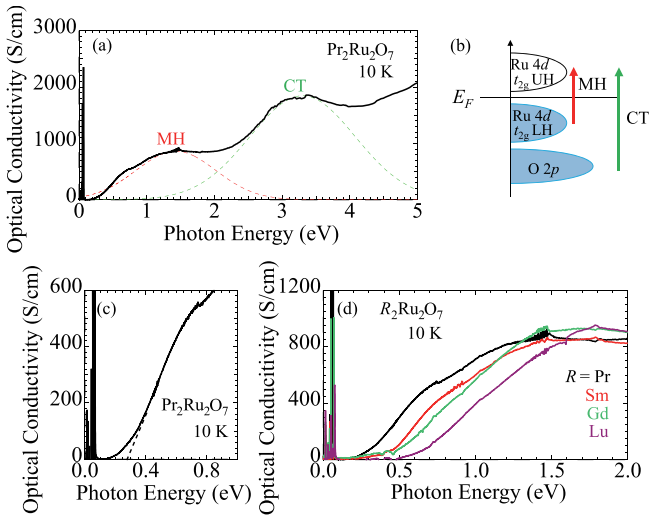

FIG. 3. (a) Optical conductivity spectra of $Pr_2Ru_2O_7$ ($R = Pr$) below the energy $\hbar\omega = 5$ eV. MH (CT) stand for Mott-Hubbard gap excitation (charge-transfer excitation). The red (green) dashed line (Lorentzian curves) is a guide to the eyes for the MH (CT) gap excitation. (b) Schematic electronic structure for $R_2Ru_2O_7$. UH (LH) stands for upper (lower) Hubbard band of the Ru-t_{2g} state. (c) Magnified view of (a) below 1 eV. The dashed line represents an extrapolating line to estimate the magnitude of the MH gap. (d) Optical conductivity spectra for $R = Pr$, Sm, Gd, Lu below 2 eV. The spiky structures of the optical conductivity spectra below 0.1 eV are all due to the optical phonon modes.

superexchange interaction ($J \propto t^2/U \propto W^2/U$) governs the magnetic ordering [19]. Thus we speculate that T_N increases with increasing r or W, reaches maximum, and then shows a rapid decrease as depicted by a dashed blue line in Fig. 2, reminiscent of the crossover from Mott type to Slater type; from the systematics of Mott gaps as described below, we anticipate that T_N would drop to zero around $r_c \sim 1.25$ Å (about 50 GPa on $R = Pr$) at which the charge gap is expected to close, as found in the canonical Mott transition system [1,19,20]. Future study employing higher-pressure application would serve to test this hypothesis.

Next, we show the optical conductivity $\sigma(\omega)$ for the $R = Pr$ compound in Fig. 3(a). There are two broad peaks locating at around 1.4 and 3.2 eV in accord with a previous work on the $R = Y$ compound [21]. The former was reasonably assigned to a Mott-Hubbard (MH) gap excitation of the Ru-4d state, while the latter to a charge transfer (CT) gap excitation from the occupied O-2p state to the upper Hubbard band of the Ru-4d state [21], as depicted in Fig. 3(b). Note that our present study does not resolve the splitting of the t_{2g} triplet by the trigonal crystal field (Δ_{tri}), whose magnitude is anticipated to be around $\Delta_{tri} \sim 0.25$ eV as shown for $Y_2Mo_2O_7$ [22], an order of magnitude smaller than the typical values of U and W which are ~2 eV and ~3 eV in the 4d oxides, respectively [23]. Figure 3(c) displays a magnified view of the optical conductivity spectrum $\sigma(\omega)$ below 1 eV; $\sigma(\omega)$ has a tail inside the gap, which may be ascribed to remnant localized in-gap states arising from unavoidable disorders or impurities. Here, we estimate the magnitude of the energy gap Δ by extrapolating the ω-linear part of $\sigma(\omega)$ [a broken line in Fig. 3(c)]. With decreasing r (or increasing U/W), the peak energy of the MH excitations in $R_2Ru_2O_7$ gradually shifts towards higher energy [Fig. 3(d)], and thereby Δ increases from 0.25 eV ($R = Pr$) to 0.60 eV ($R = Lu$), as plotted in Fig. 2. One can see that Δ decreases almost linearly along with r, as observed in other pyrochlore-type Mott-insulating oxides [18,24]. The extrapolation of the linear relation hits the hypothetical band closing $\Delta = 0$ around $r_c \sim 1.25$ Å, which corresponds to the bandwidth-control Mott transition as argued in the T_N variation with r, as shown in Fig. 2.

Next, we investigate the band-filling control Mott transition, which can be driven by substituting trivalent-R ions with divalent ions, namely, hole doping. Here we utilized Ca^{2+} for the $R = Pr$ compound and Cd^{2+} for the $R =$ Gd and Ho compounds as dopant, respectively, so that we can minimize the effect of a structural disorder stemming from the difference of A-site ionic radii in the mixed crystals. Figures 4(a)–4(c) show the temperature dependence of ρ for $(Pr_{1-x}Ca_x)_2Ru_2O_7$, $(Gd_{1-x}Cd_x)_2Ru_2O_7$, and $(Ho_{1-x}Cd_x)_2Ru_2O_7$. For $(Pr_{1-x}Ca_x)_2Ru_2O_7$, ρ decreases by several orders of magnitude with increasing the doping level x, and consequently ρ shows metallic temperature dependence down to the lowest temperature (2 K) for $x = 0.3$. On the other hand, for $(Gd_{1-x}Cd_x)_2Ru_2O_7$ and $(Ho_{1-x}Cd_x)_2Ru_2O_7$, ρ shows an upturn at low temperatures even for $x = 0.3$, although the value becomes quasimetallic, much lower than that of the undoped compounds. Concomitantly, the magnetic transitions are systematically suppressed by hole doping (not shown here) and the metallic $(Pr_{1-x}Ca_x)_2Ru_2O_7$ with $x = 0.3$ shows no longer a trace of antiferromagetic order in magnetic susceptibility, as well as $(Gd_{1-x}Cd_x)_2Ru_2O_7$ and $(Ho_{1-x}Cd_x)_2Ru_2O_7$ with $x = 0.3$. These behaviors are consistent with the results reported in Ref. [25]. We represent the optical conductivity spectra of the respective compounds in Figs. 4(d)–4(f). We show only the data measured at the lowest temperature (10 K) because the temperature dependence of $\sigma(\omega)$ is rather small apart from a thermally induced gap-filling feature and no significant change is observed through the magnetic transition for all compounds. For $(Pr_{1-x}Ca_x)_2Ru_2O_7$, as x increases, the spectral weight in the higher energy region is transferred into the MH gap region across the isosbestic point $\hbar\omega_c \sim 1.0$ eV, forms the incoherent in-gap state ($x = 0.1, 0.2$), and finally shows the broad Drude-like feature ($x = 0.3$). This behavior is ubiquitously observed in the charge-doped correlated 3d-electron systems [1]. $(Gd_{1-x}Cd_x)_2Ru_2O_7$ compounds show a similar spectral weight transfer across $\hbar\omega_c \sim 1.2$ eV except for the absence of the Drude-like coherent response. On the other hand, for $(Ho_{1-x}Cd_x)_2Ru_2O_7$, whose electronic state is characterized by larger U/W because of smaller r, the spectral weight appears not to be conserved but to increase below 2.5 eV. It is likely because the lower Hubbard (LH) band is closer to the O-2p band due to large U/W and appreciable hole doping, thereby leading to the strong hybridization of respective orbitals. In fact, the peak located at 1.8 eV for $x = 0$ gradually shifts towards lower energy with increasing x, instead of the formation of in-gap states observed for $R =$ Pr and Gd.

To discuss the evolution of the low-energy carrier dynamics quantitatively, we utilize the spectral weight represented

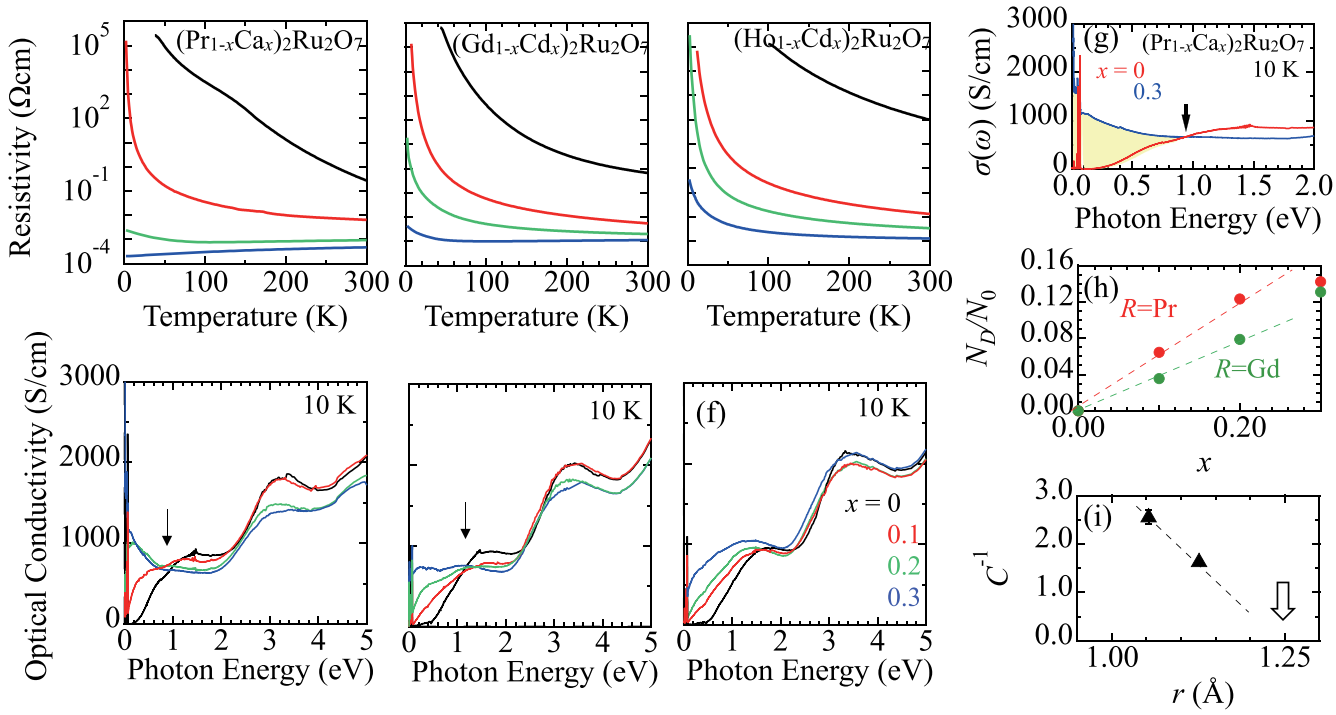

FIG. 4. (a)–(c) Temperature dependence of resistivity and (d)–(f) optical conductivity spectra of $(Pr_{1-x}Ca_x)_2Ru_2O_7$, $(Gd_{1-x}Cd_x)_2Ru_2O_7$, $(Ho_{1-x}Cd_x)_2Ru_2O_7$ for $x = 0$, 0.1, 0.2, 0.3. The downward vertical arrows in (d) and (e) indicate the isosbestic-point energies. (g) Spectral weight transfer N_D (yellow hatched region) across the isosbestic point ($\hbar\omega_c$) pointed as a black arrow. Optical conductivity spectra for $x = 0$ and 0.3 in $(Pr_{1-x}Ca_x)_2Ru_2O_7$ are displayed as an example. (h) Doping level (x) dependence of N_D of $(Pr_{1-x}Ca_x)_2Ru_2O_7$ (red circles) and $(Gd_{1-x}Cd_x)_2Ru_2O_7$ (green circles). Dashed lines presume the relation that $N_D = Cx$ in the low-doped region ($x \leqslant 0.2$). (i) C^{-1} versus R ionic radius r. The dashed lines and white arrows are guides to the eye. For the definitions of N_D and C, see text.

by the effective number of electrons,

$$N_{\rm eff}(\omega) = \frac{2m_0}{\pi e^2 N}\int_0^{\omega}\sigma(\omega')d\omega', \tag{1}$$

where m_0 is the free-electron mass and N is the number of Ru atoms per unit volume. We extract the contribution of carrier dynamics by deducing $N_D = N_{\rm eff}(\omega_c)_x - N_{\rm eff}(\omega_c)_{x=0}$, as exemplified with a yellow area in Fig. 4(g) for R = Pr with $x = 0.3$; here, ω_c is the isosbestic-point energy for the doping-induced spectral transfer and $N_{\rm eff}(\omega_c)$ for $x = 0$ corresponds to the residual component of the MH gap excitation spectrum below ω_c. We plot N_D normalized by the total spectral weight of MH plus CT excitations N_0 (estimated as $N_{\rm eff}$ at $\hbar\omega =$ 4.0 eV for $x = 0$) as a function of x in Fig. 4(h). One can see that N_D is proportional to x for $x \leqslant 0.2$ as demonstrated by broken lines in Fig. 4(h). For $x = 0.3$, on the other hand, N_D somehow deviates from the linear extrapolations. This discrepancy is partly attributable to the contribution of the higher-lying CT excitation as mentioned above.

According to previous studies on 3d transition-metal oxides such as cuprates and titanates [1,26–30], N_D is proportional to the nominal number of doped hole (x) per transition-metal ion, as described by the relation

$$N_D = Cx. \tag{2}$$

The coefficient C, representing "easiness" of doping-induced Mott transition, is closely related to the electron correlation strength U/W, as expressed by the empirical scaling relation [1,26]

$$C = [(U/W) - (U/W)_c]^{-1}. \tag{3}$$

Here $(U/W)_c$ represents a critical value of U/W at which the Mott transition occurs at zero doping ($x = 0$), i.e., the bandwidth-control MIT point.

Following the above discussion, we estimate C by fitting the obtained data in Fig. 4(h) below $x = 0.2$ and plot the inverse of C as a function of r in Fig. 4(i). Given that C^{-1} is in proportion to r as demonstrated in Ref. [26], C^{-1} appears to go towards 0 at around $r_c \sim 1.25$ Å; this point coincides with the hypothetical bandwidth-control MIT point where the charge gap appears to close, as already shown in Fig. 2. On the whole, these findings are in good agreement with the theoretical results for the Hubbard model [28], indicating that the pyrochlore ruthenates in the relatively weak electron correlation regime (r being larger than that of R = Gd) and the low-doping region of $x < 0.3$ can be well described within the framework of the Hubbard model. It should be noted that, for highly-hole-doped ($x \geqslant 0.3$) and larger-(U/W) compounds which are out of this framework, the Ru-4d states seem to hybridize strongly with O-2p states or, in other words, the O-2p hole character becomes prominent; this feature potentially may give rise to novel phenomena such as unique magnetism or superconductivity [31–33]. Mazin and Singh, who theoretically studied the magnetic properties in the context of Stoner theory, suggest that the mixing of O-2p states plays a significant role in the magnetism in Ru-based perovskites [34]. It

is also worth mentioning other $A_2^{3+}Ru_2^{4+}O_7$ compounds such as metallic $Bi_2Ru_2O_7$ and $Tl_2Ru_2O_7$. Previous spectroscopic studies and *ab initio* calculations suggest that the hybridizations between Ru-4*d* states and unoccupied Bi-6*d* or Tl-6*s* states are not negligible in these materials, resulting in the substantial screening of U [35]. Therefore, a further study which goes beyond the present work based on the canonical Mott-Hubbard model should be necessary to understand exotic electronic properties in these materials. Incidentally, as far as the Mott transition or the MIT is concerned in the present Ru 4*d*-electron-based pyrochlores, the impact of the relativistic spin-orbit coupling λ and the multiorbital effect mediated by Hund's coupling J, such as $\lambda \sim 0.2$ eV [36] and $J \sim 0.5$ eV [37], are not clearly visible in the present optical study, yet presumably emerge in the low-energy charge dynamics when the 4*d* conduction electrons become spin polarized, e.g., via coupling with R-4f moments, in higher-doping regime.

In summary, we investigate the charge dynamics of $R_2Ru_2O_7$ and their hole-doped compounds in terms of optical conductivity spectra. We exploit the pyrochlore A-site chemical substitution and high-pressure application to tune effective one-electron bandwidth and band filling precisely, so that we can examine the critical Mott transitions. With increasing the hole-doping level, the resistivity decreases significantly while the charge gap in the optical conductivity spectrum close systematically. We quantitatively analyze the optical conductivity spectra to confirm that the transfer of the spectral weight from the above-gap photon-energy region to the in-gap region is intimately related to the variation of R ionic radius (effective bandwidth), which is in good agreement with the canonical systematics known for 3*d* Mott systems. The above analysis can point to the identical critical value of U/W for bandwidth-control Mott transition in the undoped parent compounds, which would be able to be reached by the application of high pressure ($\sim$50 GPa) on $Pr_2Ru_2O_7$, beyond the chemical modification of R.

We thank R. Arita, S. Sakai, and Y. Nomura for fruitful discussions and Y. Kaneko and A. Kikkawa for helpful advice about crystal growth. This work was supported by the Japan Society for the Promotion of Science (KAKENHI; Grant No. 19K14647) from the MEXT, and by CREST (Grants No. JPMJCR16F1 and No. JPMJCR1874) from Japan Science and Technology Agency.

[1] M. Imada, A. Fujimori, and Y. Tokura, Rev. Mod. Phys. **70**, 1039 (1998).
[2] P. A. Lee, N. Nagaosa, and X.-G. Wen, Rev. Mod. Phys. **78**, 17 (2006).
[3] Y. Tokura, Rep. Prog. Phys. **69**, 797 (2006).
[4] W. W. Krempa, G. Chen, Y. B. Kim, and L. Balents, Annu. Rev. Condens. Matter Phys. **5**, 57 (2014).
[5] K. Ueda, T. Oh, B.-J. Yang, R. Kaneko, J. Fujioka, N. Nagaosa, and Y. Tokura, Nat. Commun. **8**, 15515 (2017).
[6] N. Taira, M. Wakeshima, and Y. Hinatsu, J. Phys.: Condens. Matter **11**, 6983 (1999).
[7] M. Ito, Y. Yasui, M. Kanada, H. Harashina, S. Yoshii, K. Murata, M. Sato, H. Okumura, and K. Kakurai, J. Phys. Chem. Solids **62**, 337 (2001).
[8] J. S. Gardner, M. J. P. Gingras, and J. E. Greedan, Rev. Mod. Phys. **82**, 53 (2010).
[9] J. N. Reimers, A. J. Berlinsky, and A.-C. Shi, Phys. Rev. B **43**, 865 (1991).
[10] J. Gurgul, M. Rams, Z. Swiatkowska, R. Kmiec, and K. Tomala, Phys. Rev. B **75**, 064426 (2007).
[11] J. van Duijn, K. H. Kim, N. Hur, R. Ruiz-Bustos, D. T. Adroja, F. Bridges, A. Daoud-Aladine, F. Fernandez-Alonso, J. J. Wen, V. Kearney, Q. Z. Huang, S.-W. Cheong, T. G. Perring, and C. Broholm, Phys. Rev. B **96**, 094409 (2017).
[12] T. Munenaka and H. Sato, J. Phys. Soc. Jpn. **75**, 103801 (2006).
[13] Y. Y. Jiao, J. P. Sun, P. Shahi, Q. Cui, X. H. Yu, Y. Uwatoko, B. S. Wang, J. A. Alonso, H. M. Weng, and J.-G. Cheng, Phys. Rev. B **98**, 075118 (2018).
[14] A. Yamamoto, P. A. Sharma, Y. Okamoto, A. Nakao, H. A. Katori, S. Niitaka, D. Hashizume, and H. Takagi, J. Phys. Soc. Jpn. **76**, 043703 (2007).
[15] N. Mori, H. Takahashi, and N. Takeshita, High Press. Res. **24**, 225 (2004).
[16] K. Ueda, J. Fujioka, C. Terakura, and Y. Tokura, Phys. Rev. B **92**, 121110(R) (2015).
[17] S.-W. Cheong, H. Y. Hwang, C. H. Chen, B. Batlogg, L. W. Rupp, and S. A. Carter, Phys. Rev. B **49**, 7088(R) (1994).
[18] K. Ueda, J. Fujioka, and Y. Tokura, Phys. Rev. B **93**, 245120 (2016).
[19] J. Goodenough, J. Longo, and J. Kafalas, Mat. Res. Bull. **3**, 471 (1968).
[20] A. Georges, G. Kotliar, W. Krauth, and M. J. Rozenberg, Rev. Mod. Phys. **68**, 13 (1996).
[21] J. S. Lee, Y. S. Lee, T. W. Noh, K. Char, J. Park, S.-J. Oh, J.-H. Park, C. B. Eom, T. Takeda, and R. Kanno, Phys. Rev. B **64**, 245107 (2001).
[22] I. V. Solovyev, Phys. Rev. B **73**, 155117 (2006).
[23] A. Georges, L. Medici, and J. Mravlje, Annu. Rev. Condens. Matter Phys. **4**, 137 (2013).
[24] I. Kezsmarki, N. Hanasaki, K. Watanabe, S. Iguchi, Y. Taguchi, S. Miyasaka, and Y. Tokura, Phys. Rev. B **73**, 125122 (2006).
[25] S. Yoshii, K. Murata, and M. Sato, J. Phys. Chem. Solids **62**, 129 (2001).
[26] T. Katsufuji, Y. Okimoto, and Y. Tokura, Phys. Rev. Lett. **75**, 3497 (1995).
[27] M. Jarrell, J. K. Freericks, and T. Pruschke, Phys. Rev. B **51**, 11704 (1995).
[28] E. Dagotto, A. Moreo, F. Ortolani, D. Poilblanc, and J. Riera, Phys. Rev. B **45**, 10741 (1992).
[29] Y. Okimoto, T. Katsufuji, Y. Okada, T. Arima, and Y. Tokura, Phys. Rev. B **51**, 9581 (1995).
[30] K. Morikawa, T. Mizokawa, A. Fujimori, Y. Taguchi, and Y. Tokura, Phys. Rev. B **54**, 8446 (1996).
[31] Y. Maeno, S. Kittaka, T. Nomura, S. Yonezawa, and K. Ishida, J. Phys. Soc. Jpn. **81**, 011009 (2011).

[32] G. Cao, S. McCall, M. Shepard, J. E. Crow, and R. P. Guertin, Phys. Rev. B **56**, 321 (1997).

[33] H. Suzuki, H. Gretarsson, H. Ishikawa, K. Ueda, Z. Yang, H. Liu, H. Kim, D. Kukusta, A. Yaresko, M. Minola, J. A. Sears, S. Francoual, H. C. Wille, J. Nuss, H. Takagi, B. J. Kim, G. Khaliullin, H. Yavaş, and B. Keimer, Nat. Mater. **18**, 563 (2019).

[34] I. I. Mazin and D. J. Singh, Phys. Rev. B **56**, 2556 (1997).

[35] J. S. Lee, S. J. Moon, T. W. Noh, T. Takeda, R. Kanno, S. Yoshii, and M. Sato, Phys. Rev. B **72**, 035124 (2005).

[36] C. G. Fatuzzo, M. Dantz, S. Fatale, P. Olalde-Velasco, N. E. Shaik, B. Dalla Piazza, S. Toth, J. Pelliciari, R. Fittipaldi, A. Vecchione, N. Kikugawa, J. S. Brooks, H. M. Rønnow, M. Grioni, C. Rüegg, T. Schmitt, and J. Chang, Phys. Rev. B **91**, 155104 (2015).

[37] M. Cuoco, C. Noce, and A. Romano, Phys. Rev. B **57**, 11989 (1998).